Research Article

Journal of Environmental Nanotechnology

Green Engineering of Surfactant-assisted Nanosilica Dispersion in Alkaline Cementitious Systems Using Chitosan

J. Vignesh[1], Vidhya Lakshmi Sivakumar[1*], A. Kandasamy[1] and Mahmoud Al Khazaleh[2]

[1]Department of Civil Engineering, Saveetha School of Engineering, Saveetha Institute of Medical and Technical Sciences, Chennai, TN, India
[2]Department of Civil Engineering, Dean of Munib and Angela Masri Engineering Faculty, Aqaba University of Technology, AQ, Jordan
Received: 03.08.2025 Accepted: 15.09.2025 Published: 30.09.2025
*vidhyalakshmis.sse@saveetha.com

ABSTRACT

Achieving uniform dispersion of nanosilica (NS) is critical for enhancing the performance of cementitious composites. But conventional dispersants such as polycarboxylate ether (PCE) pose environmental and economic drawbacks. This study investigates a combined ultrasonication and chitosan stabilization approach as a sustainable strategy to disperse NS. Multi-scale analyses were performed to evaluate its influence on hydration kinetics, phase composition, pore structure, microstructural morphology, and macro-scale properties, including compressive strength, ultrasonic pulse velocity (UPV), and electrical resistivity, relative to PCE-treated NS and plain Ordinary Portland Cement (OPC). The synergistic action of ultrasonication and chitosan enhanced NS dispersion, accelerated cement hydration, and promoted pozzolanic reactions, fostering denser C–S–H gel formation and reducing calcium hydroxide content. The resulting microstructure exhibited reduced critical, average, and median pore diameters by 23.2%, 32.3%, and 41.7%, respectively, and total porosity decreased by 21.3% compared with OPC. These structural refinements translated into improved performance: at 90 days, compressive strength, UPV, and resistivity increased by 5.0%, 7.1%, and 12.1%, respectively, over PCE–NS. Furthermore, chitosan's water-retention and crack-mitigation abilities enhanced internal curing and long-term durability. Overall, the combined ultrasonication–chitosan strategy provides a green, biodegradable, and highly effective dispersant approach, enabling the fabrication of durable, high-performance cementitious composites.

Keywords: Nanosilica dispersion; Polycarboxylate ether (PCE); Cement hydration; Pozzolanic reaction; C–S–H gel formation.

1. INTRODUCTION

Cement-based composites are extensively used in civil engineering projects worldwide due to their low cost, ease of raw material procurement, and favorable properties such as high compressive strength, stiffness, and durability (Jonnala *et al*. 2024). However, they also exhibit notable drawbacks, including brittleness, limited tensile capacity, and degradation under aggressive environments, which reduce service life and raise maintenance costs (Zhao *et al*. 2022). To address these issues, the incorporation of nanomaterials into cementitious systems has gained attention. With their high surface area and reactivity, nanomaterials can induce micro- to nano-scale modifications that enhance performance (Du *et al*. 2019; Jafarbeglou *et al*. 2015). Such refinements open avenues for next-generation cement-based materials with improved resilience and durability (Song and Li, 2021; Safiuddin *et al*. 2014).

Among these, nanosilica (NS), an amorphous form of SiO_2 with particle sizes typically 5–100 nm, has been widely studied. Depending on the synthesis route (sol-gel, precipitation, or fumed methods), NS exhibits spherical or aggregated morphology, high surface area, abundant hydroxyl groups, and strong pozzolanic reactivity (Saleh *et al*. 2015; Bai *et al*. 2021; Kandasamy *et al*. 2025a). These features enable NS to actively participate in hydration, improving the microstructure, mechanical strength, and durability of cementitious composites (Hou *et al*. 2015; Khan *et al*. 2022; Golewski, 2022). Nanosilica is known to accelerate hydration kinetics and increase early-age strength by refining pore structure (Chong *et al*. 2013; Lu *et al*. 2020). For instance, additions up to 10 wt% NS have enhanced mechanical properties (Biricik and Sarier, 2014), while synergistic use with nano alumina has achieved 35% strength improvement and 25% porosity reduction after 120 days compared to plain OPC (Tsampali *et al*. 2019; Jahangir and Kazemi, 2014).

Despite these benefits, achieving uniform dispersion of NS in alkaline cement pore solutions remains a major challenge. The abundance of Na^+, K^+, Ca^{2+}, and hydroxide ions promotes particle agglomeration by charge screening and interparticle attraction, reducing available surface area and reactivity (Yang *et al*. 2023). Thus, effective dispersion is critical to maximize NS performance. Reported approaches include ultrasonication, surface treatment, and the use of

dispersants. Conventionally, polycarboxylate ether (PCE) superplasticizers are combined with ultrasonication to improve suspension stability (Ren *et al*. 2020). Alternatively, some studies employ direct mixing with surfactants or even dry blending, though such practices often neglect essential dispersion requirements (Iqbal *et al*. 2024).

An eco-friendly strategy to stabilize the dispersion of NS involves the surface adsorption of biopolymers such as chitosan. This technique improves the stability of the dispersion and enhances the environmental compatibility of the additive system (Nicolle *et al*. 2021). Chitosan, a cationic biopolymer, possesses excellent film-forming capability, pH tolerance, and biocompatibility (Aranaz *et al*. 2021). It can adsorb onto the NS surface *via* electrostatic interactions between its protonated amine groups and negatively charged silanol groups, forming a stabilizing layer that hinders particle aggregation. Biopolymers like chitosan can function *via* both steric and electrostatic stabilization mechanisms, depending on their ionic character (Tyukova *et al*. 2014). Cationic biopolymers such as chitosan are particularly suited for high-pH environments due to their capacity to maintain dispersion stability under alkaline conditions (Bi *et al.* 2020). Chitosan stands out as a natural and versatile alternative to synthetic surfactants for dispersing nanoparticles in cement systems. Its unique structure, rich in amine and hydroxyl groups, allows it to bond effectively with both nanoparticles and calcium ions, forming stable coatings that keep particles well-dispersed even in cement pore solutions. Unlike many synthetic surfactants that often interfere with hydration or retard setting, chitosan is gentle on the cement matrix and even promotes better integration with hydration products through hydrogen bonding and mild ionic interactions. Another advantage is its pH-responsive nature. While it disperses nanoparticles efficiently in mildly acidic or neutral suspensions, it becomes more compatible under alkaline conditions. Beyond performance, chitosan is renewable, biodegradable, and non-toxic, aligning with the growing push for greener construction materials. It also avoids the foaming and excess air entrainment issues that can occur with traditional surfactants.

Importantly, chitosan is also compatible with cement chemistry, having been shown to minimally interfere with hydration kinetics while contributing to improved workability, reduced bleeding, and microstructural refinement. From a sustainability standpoint, the use of chitosan as a green surfactant eliminates the need for synthetic dispersants, aligning with eco-friendly construction practices. Although some previous works have reported on the colloidal stabilization of NS using natural polymers in aqueous media (Singh *et al.* 2024), comprehensive studies on how chitosan-modified NS influences cementitious systems at both micro- and macro-scales remain sparse. Investigating this green engineering strategy not only offers a pathway to better dispersion and enhanced performance but also contributes to reducing the environmental footprint of nanomodified cement composites. Hence, the potential of chitosan as a bio-based surfactant for NS dispersion in cementitious systems requires in-depth exploration, particularly about its effects on hydration, pore structure, and long-term durability under aggressive exposure conditions (Kandasamy *et al* 2025c).

Building upon the preceding discussion, the central objective of this experiment is to study the influence of chitosan-stabilized nanosilica on both the microstructural and macroscopic properties of cementitious composites, in direct comparison with systems incorporating PCE-dispersed nanosilica. Polycarboxylate ether has long been utilized as a stabilizer and surfactant to enhance the dispersion of nanoparticles within cementitious environments, as documented in numerous prior studies (Wang *et al*. 2023a; Liu *et al.* 2022; Feng *et al.* 2020). In this work, the microstructural characteristics of NS-modified cement mortars were thoroughly examined using techniques such as X-ray diffraction (XRD) to monitor hydration product formation, thermogravimetric analysis (TGA) to quantify bound phases, and mercury intrusion porosimetry (MIP) for pore structure characterization. Scanning Electron Microscopy (SEM) was used to study the morphology of the composites. To assess macro-level performance, mechanical and durability-related tests were conducted, including compressive strength, ultrasonic pulse velocity (UPV), and electrical resistivity measurements at multiple curing ages. The findings of this investigation aim to establish a sustainable and efficient alternative to chemical surfactants for nanosilica dispersion, thereby advancing the development of eco-friendly, high-performance cementitious materials through improved nanoparticle integration at both the nano- and macro-scales.

2. EXPERIMENTAL METHODOLOGY

2.1 Materials Used

Ordinary Portland Cement (OPC) 43 Grade, conforming to the IS 8112:2013 specification (BIS, 2013), was adopted with a measured density of 3.15 g cm^{-3} and a Blaine fineness of 3450 cm^2/g^{-1}. The nanosilica used was an amorphous silica nanopowder sourced from Sigma-Aldrich. It exhibited an average particle size of 15–20 nm, a high specific surface area of approximately 200 m^2/g^{-1}, and a bulk density of 2.2 g cm^3.

The amorphous nature of the NS was confirmed through X-ray diffraction (XRD) analysis (Fig. 1), which aligned well with the previous findings (Naddaf *et al*. 2020). The chemical compositions of OPC and NS were

determined using X-ray fluorescence (XRF) *via* a PANalytical Axios spectrometer, and the results are provided in Table 1. The mineralogical composition of OPC was estimated using the Bogue equations, with calculated values listed in Table 2. Standard natural river sand was used as fine aggregate, in accordance with IS 650:1991 (BIS, 1991) and IS 383:2016 (BIS, 2016). To achieve stable colloidal dispersion of NS in the high-alkalinity cementitious matrix, a chitosan biopolymer procured from Sigma-Aldrich was employed as a green surfactant owing to its cationic nature, pH tolerance, and bio-compatibility. For comparison, a PCE-based superplasticizer was used as a conventional chemical dispersant. The physicochemical properties of both chitosan (Ch) and PCE surfactants are summarized in Table 3 to support the comparison of their effectiveness in stabilizing NS dispersions in cementitious systems.

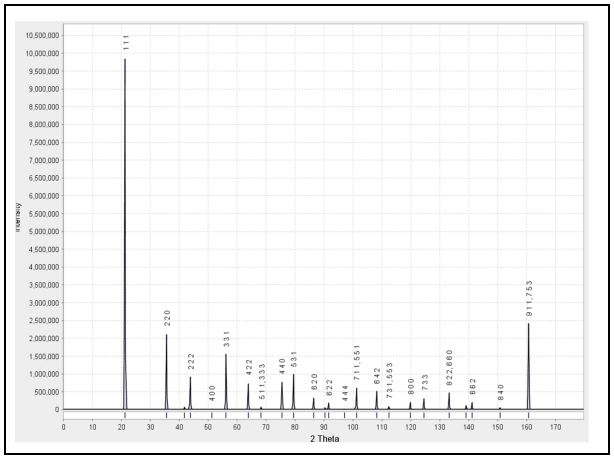


Fig. 1: XRD patterns of nanosilica showing its amorphous nature and characteristic broad hump around 2θ ≈ 22–23°

Table 1. Chemical composition of OPC and NS

Material	SiO_2	Al_2O_3	Fe_2O_3	CaO	MgO	SO_3	K_2O	Loss on Ignition (%)
OPC	21.5	4.8	3.1	63.2	2.5	2.6	0.8	1.5
Nano-silica	99.2	0.3	0.1	0.1	—	—	—	0.5

Table 2. Mineral compositions of OPC

Mineral	Alite (C_3S)	Belite (C_2S)	Aluminate (C_3A)	Ferrite (C_4AF)
Content (wt. %)	52.0	23.0	7.5	8.5

2.2. Preparation of Chitosan-nanosilica and PCE-nanosilica Suspension

A combined physicochemical dispersion technique was employed to prepare the suspensions. Initially, NS powder was dispersed in deionized water (pH ≈ 6.8) and subjected to ultrasonication using a probe-type ultrasonic processor (400 W, 20 kHz) equipped with a 13 mm titanium tip. Sonication was carried out for 15 minutes. To prevent thermal degradation or agglomeration during the process, the suspension was kept in an ice-cold water bath. Following sonication, the chitosan biopolymer was introduced into the dispersion and stirred using a high-speed mechanical stirrer at 1000 rpm for 2 minutes to ensure homogeneous mixing. The PCE–NS suspension was prepared based on the procedure reported by previous researchers, wherein the PCE surfactant was directly added to the NS dispersion under identical sonication and mixing conditions.

Table 3. Characteristics of the surfactants used

Surfactant	Density (g/cm^3)	Physical State	Color
Chitosan	1.42	Powder (solid)	Off-white to pale yellow
PCE	1.01	Liquid (aqueous)	Clear yellow to amber

Table 4. Mix proportions of samples

Mix Code	OPC (kg/m^3)	Nano-silica (kg/m^3)	Water (kg/m^3)	Standard Sand (kg/m^3)	Chitosan (% Binder Mass)	PCE (% Binder Mass)
CTRL	542.50	–	263.1	1 356.3	–	–
NS–Ch	531.65	10.85	265.0	1 356.3	0.3 %	–
NS–PCE	531.65	10.85	263.1	1 356.3	–	0.3 %

2.3. Mix Procedure

Table 4 outlines the control and comparison groups used in the study. The water-to-binder ratio (w/b) and sand-to-binder ratio were maintained at 0.485 and 2.5, respectively, with the binder defined as the combined mass of OPC and nanosilica. The dosage of chitosan or PCE surfactant was fixed at 0.3% by weight of the binder, in line with effective concentrations identified in earlier studies (Li *et al*. 2023a; Qian *et al*. 2018). The prepared chitosan-NS or PCE–NS suspensions were mixed with OPC and standard graded sand in a laboratory mortar mixer. The mixing protocol adhered to the IS 4031 (Part 6):1988 (Bureau of Indian Standards, 1988) procedure, which is equivalent to ASTM C305 (American Society for Testing and Materials, 2020). Fresh mortar was cast into 50 mm cube molds and 40 × 40 × 160 mm prism molds. To eliminate entrapped air and ensure proper compaction, the molds were vibrated on a standard vibrating table at 25 Hz for 2 minutes. Specimens were demolded after 24 hours and shifted to a curing chamber maintained at 27 ± 2 °C and relative humidity above 95% until the designated testing ages.

2.4 Methods of Testing

2.4.1 Micro-level Assessments

2.4.1.1 X-ray Diffraction (XRD)

The identification of crystalline hydration products was carried out using an Analytical X'Pert PRO X-ray diffractometer. For this analysis, powdered samples were collected from the central zone of 90-day cured cubic specimens following compressive strength testing. These fragments were ground and subsequently oven-dried under vacuum at 23 ± 2 °C for 72 hours to eliminate any residual moisture before XRD testing. Chitosan crystal size was also calculated using the Debye–Scherrer equation (Mustapha *et al*. 2019), based on FWHM values extracted from three key CH peaks at 18.0°, 34.1°, and 50.8°. These peaks were analyzed using Origin software to determine 2θ and FWHM values, which were then applied to the Debye–Scherrer formula:

$$D = \frac{K.\lambda}{\beta.\cos\theta} \quad \ldots (1)$$

Here, D denotes the crystallite size in nanometers (nm), κ is the shape factor (commonly taken as 0.9), λ represents the X-ray wavelength (1.5406 Å for Cu Kα radiation), β is the full width at half maximum expressed in radians, and θ corresponds to the Bragg diffraction angle.

2.4.1.2 Thermogravimetric Analysis (TGA)

Thermal decomposition and mass loss behavior, indicative of hydration and pozzolanic activity, were analyzed using a TA Instruments SDT Q600 thermogravimetric analyzer (USA). Approximately 15 mg of finely ground cementitious paste from the 90-day nanosilica-modified mortar specimens was subjected to a heating cycle from 50 °C to 1000 °C at a constant rate of 10 °C/min under an inert argon atmosphere. Sample preparation followed the same drying and grinding procedures as used for the XRD tests. Ch, C–S–H, and non-evaporable water contents were derived from the TG data to evaluate hydration and pozzolanic activity. Mass loss between 400–500 °C ($WL_{400\text{-}500}$ °C) was used to compute Ch content:

$$Ch\ (\%) = WL_{400\text{-}500}\ (\%) \times (m(Ch) / m(H_2O))$$

where m(Ch) = 74.09 g/mol and $m(H_2O)$ = 18.02 g/mol. Water loss from 150–400 °C ($WL_{150\text{-}500}$ °C) represents C–S–H gel dehydration and was converted to C–S–H content using:

$$C\text{–}S\text{–}H\ (\%) = WL_{150\text{-}400}\ (\%) \times (2 \times m(C\text{–}S\text{–}H) / 2.1 \times m(H_2O))$$

with m(C–S–H) = 193.26 g/mol, assuming equilibrium $C_{1.7}SH_{2.1}$ composition (Scrivener *et al.* 2016; Jain and Neithalath, 2009; Jiang *et al.* 2021). Non-evaporable water was determined as mass loss below 150 °C minus that above 1000 °C (Escalante-Garcia, 2003; Li *et al*., 2023).

2.4.1.3 Mercury Intrusion Porosimetry (MIP)

The pore structure and total porosity of the 90-day hardened cement mortars were determined using Mercury Intrusion Porosimetry (MIP) with a Quantachrome PoreMaster (USA). Samples were obtained from fractured portions of previously tested cubes, oven-dried at 50 °C to remove free water, and then subjected to intrusion analysis under pressures ranging from 0.003 to 200 MPa. This allowed quantification of pore diameters between ~5 nm and 100 µm, covering both capillary and macropore ranges. The cumulative intrusion curves were used to calculate total porosity, while differential intrusion profiles provided pore size distribution. This method gave reliable insight into the refinement of pore structure induced by NS and biopolymer modifications.

2.4.1.4 Scanning Electron Microscopy (SEM)

The surface morphology and microstructural characteristics of the 90-day nanosilica-modified mortars were examined using a JEOL JSM-7610F field emission scanning electron microscope (Japan). Small fragments measuring approximately 5 × 5 × 2 mm^3 were collected from the fractured portions of compressive test specimens. Before imaging, samples were vacuum-dried at 23 ± 2 °C for 72 hours, followed by careful polishing and coating with a thin layer of platinum to improve electrical conductivity. Imaging was performed at an accelerating voltage of 15–20 kV, with a working

distance of 10 ± 2 mm, providing high-resolution micrographs for detailed observation of the cementitious matrix, nanosilica dispersion, and hydration product morphology.

2.4.2 Macro-level Assessments

2.4.2.1 Compressive Strength

Compressive strength measurements were performed on 50 mm cubic mortar specimens at curing ages of 28 and 90 days. A calibrated compression testing machine with a maximum capacity of 3000 kN was used, applying a constant loading rate of 1.5 kN/s. The procedure followed the guidelines of IS 4031 (Part 6):1988, which outlines the standard method for evaluating the compressive strength of cement mortar cubes. Tests were conducted under controlled and uniform loading to monitor the progression of strength with curing time accurately.

2.4.2.2 Ultrasonic Pulse Velocity (UPV)

Ultrasonic pulse velocity (UPV) measurements were performed on prismatic mortar specimens of 40 × 40 × 160 mm, cured for 28 and 90 days. The testing procedure followed is IS 13311 (Part 1):1992, which outlines non-destructive evaluation of concrete using ultrasonic waves. A Sundoo USN-55 ultrasonic testing instrument was employed, and both ends of each specimen were coated with coupling gel to ensure proper contact between the transducer and receiver for accurate pulse transmission.

2.4.2.3 Electrical Resistivity

The electrical resistivity of mortar specimens was evaluated at 28 and 90 days using the two-electrode method in line with procedures described in relevant research (Yim *et al.* 2017). The prismatic specimens (40 mm × 40 mm × 160 mm), in a saturated surface-dry state, were placed between brass plate electrodes (60 mm × 60 mm × 1 mm). A 1 kHz AC signal was applied using a digital resistivity meter, and the resistance was recorded. To enhance contact, wet sponges were applied at both ends. The bulk electrical resistivity (ρ) was calculated using the following relation:

$$\rho = (R \times A) / l \quad \ldots (2)$$

In this equation, rho (ρ) denotes the electrical resistivity in kilo-ohm centimeters (kΩ·cm), and R represents the measured resistance in kilo-ohms (kΩ). Here, A represents the cross-sectional area of the specimen in square centimeters (cm^2), and l denotes the distance between the electrodes in centimeters (cm). For the evaluation of macroscopic and microscopic properties, six and three specimens per group were tested, respectively, and the results presented correspond to the mean values obtained from these measurements.

3. RESULTS AND DISCUSSION

3.1 Microscale Morphology

3.1.1 XRD Analysis

Fig. 2 displays the normalized XRD patterns for specimens cured for over 90 days. The most prominent reflection linked with the C_3S phase appeared at 2θ ≈ 29.5°, corresponding to the (422) crystallographic plane. Interestingly, this C_3S peak was absent in the Ch–NS–OPC specimen, whereas it remained visible, though diminished in intensity, in the NS–PCE–OPC sample compared to the reference OPC mixture. The retention of the C_3S peak in the OPC control indicates the persistence of unhydrated clinker minerals even after 90 days of curing. Conversely, the disappearance of this peak in the Ch–NS–OPC sample suggests that the enhanced dispersion of nanoparticles fostered more complete cement hydration (Korayem *et al.* 2017; Rupasinghe *et al*. 2017), leading to full participation of clinker constituents in the hydration process.

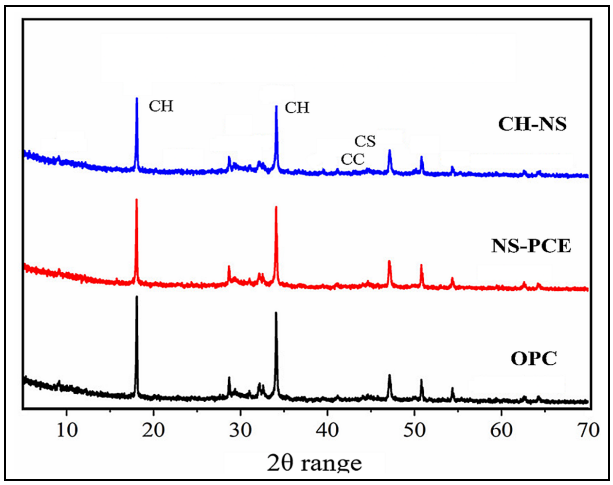


Fig. 2: XRD analyses of control (OPC), nanosilica-PCE, and chitosan-nanosilica cement specimens at 90 days

The dominant SiO_2 peak, corresponding to the (101) plane, was identified near 2θ ≈ 26.6°. The intensity of this quartz reflection remained relatively unchanged across all cementitious formulations. This constancy suggests that the incorporation of nano-silica or chitosan-modified NS does not significantly affect the quartz peak intensity. Since quartz is known to be inert in pozzolanic reactions, it primarily functions as a filler phase in these systems (Wu *et al.* 2020). The principal peak of AFt was found at 2θ ≈ 9.1°, associated with the (100) plane. A substantial increase in AFt peak intensity was observed in the Ch–NS–OPC mixture compared to the plain OPC and NS–PCE–OPC mixtures, respectively. This improvement is attributed to the synergistic presence of additional alumina from the chitosan-functionalized nano-silica and the inherent C_3A phase in cement (Rath *et al.* 2025).

Furthermore, the major peaks of calcium hydroxide (CH), a critical crystalline product of cement hydration were detected at approximately 2θ ≈ 18.0°, 34.1°, and 50.8°, aligning with the (001), (101), and (110) planes, respectively. Among these, the 18.0° peak is widely utilized as an indicator of hydration progress and pozzolanic activity (Heikal *et al.* 2013). The CH peak intensities in the Chitosan–NS–OPC mix were lower in comparison to the OPC control and NS–PCE–OPC mixtures. Specifically, at 18.0°, the CH peak intensity in the chitosan-modified sample declined relative to OPC and NS–PCE–OPC, respectively. This reduction indicates the consumption of CH due to secondary pozzolanic reactions, leading to the formation of binding gels such as calcium silicate hydrates (C–S–H), (C–A–S–H), and (C–A–H) (Xu *et al.* 2016).

Incorporating chitosan-functionalized nanosilica in OPC significantly reduced CH crystal size, with the Chitosan–NS–OPC sample showing a 30.2% and 21.7% decrease compared to OPC and NS–PCE–OPC, respectively. This downsizing of CH crystals enhances interfacial bonding with the C–S–H gel, as further discussed in Section 3.1.4 (Wang *et al.* 2019). Such microstructural refinement contributes to improved material cohesion and elevates overall mechanical performance, which will be elaborated in Section 3.2. In conclusion, replacing part of OPC with uniformly dispersed chitosan–nano-silica not only lowers CH content *via* pozzolanic reactivity but also improves the cement matrix by reducing CH crystal size, promoting a denser and more cohesive microstructure.

3.1.2 Thermogravimetric (TG) and Derivative Thermogravimetric (DTG) Analysis

Because XRD cannot directly quantify amorphous hydration products, a thermogravimetric (TG) and derivative thermogravimetric (DTG) approach was adopted to yield quantitative insight into cement hydration. Fig. 3 summarizes the TG mass remaining and DTG peak temperatures for OPC, NS–PCE–OPC, and Chitosan–NS–OPC specimens after 90 days of curing. In all DTG traces, two principal endothermic events appear: one below 150 °C, corresponding to loss of free and bound water from C–S–H gel and AFt (Zhao *et al*. 2017); and another between 400 °Cand 500 °C, indicating dehydroxylation of portlandite (CH) to CaO and H_2O (Stepkowska, 2005).

Closer examination shows that the Chitosan–NS–OPC mix exhibits a sharper, higher-temperature low-end peak at 110 °C compared to 100 °C and 105 °°C for OPC and NS–PCE–OPC, respectively, signifying increased and more strongly bound C–S–H and AFt formation. Its CH dehydroxylation peak is weaker and shifts to 460 °C *versus* 480 °C and 470 °C in OPC and NS–PCE–OPC, reflecting enhanced CH consumption via pozzolanic reaction. Both NS–PCE–OPC and Chitosan–NS–OPC show a minor DTG shoulder around 300 °C, attributed to aluminum hydroxide ($Al(OH)_3$) dehydroxylation (Maach *et al.* 2021), suggesting formation of calcium aluminosilicate and aluminate hydrates (C–A–S–H, C–A–H) due to higher C_3A reactivity (Joseph *et al.* 2019). Notably, no significant DTG peaks are observed in the 600–800 °C range, indicating negligible $CaCO_3$ decomposition and minimal carbonation, consistent with previous studies (Li *et al.* 2021).

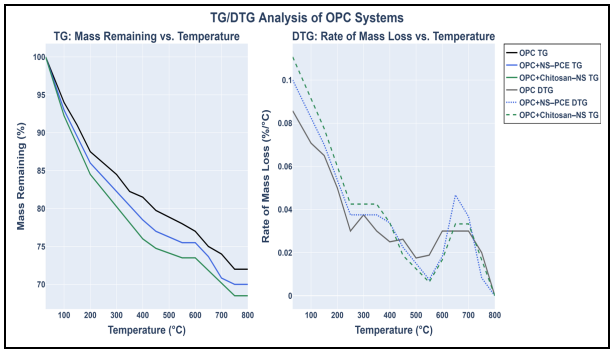


Fig. 3: TG/DTG curves of mixed specimens

As illustrated in Fig. 4, OPC retains 81.50 % mass at 400 °C and 78.88 % at 500 °C, while NS–PCE–OPC retains 78.50 % and 76.25 %, and Chitosan–NS–OPC retains only 76.00 % and 74.13 %, confirming greater CH consumption and higher bound water in the modified mixes. Ordinary Portland Cement exhibits 2.62 % CH decomposition, indicating continuous hydration of C_3S/C_2S. NS–PCE–OPC shows CH decomposition reduced to 2.25 %, reflecting pozzolanic uptake by surface-modified nanosilica (Ren *et al.* 2020). Chitosan–NS–OPC drops further to 1.87 % CH, demonstrating superior dispersion and reactivity of chitosan-grafted nanoparticles (Rahmani *et al.* 2022). Similarly, C–S–H content increases from 9.50 % in OPC to 11.00 % and 12.38 % in NS–PCE–OPC and Chitosan–NS–OPC, respectively. Non-evaporable water is also highest in Chitosan–NS–OPC (11.62 %), confirming accelerated hydration kinetics.

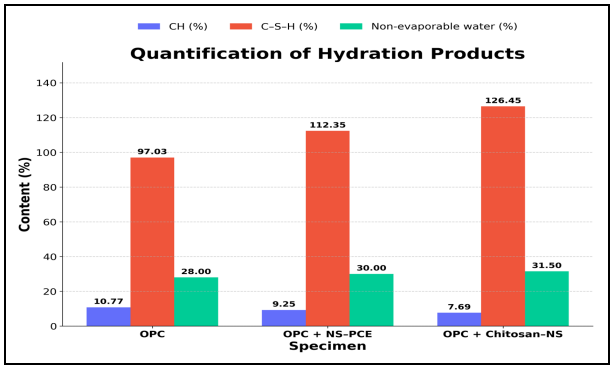


Fig. 4: CH, C–S–H, and non-evaporable water content of mix specimens

These enhancements stem from several factors: dispersed nanosilica provides abundant nucleation sites for C–S–H; its intrinsic pozzolanic reactivity consumes CH to form secondary C–S–H (Dong *et al.* 2022; Kim *et al*. 2014); while chitosan biopolymer further minimizes water evaporation during curing, promoting hydration (Yehia *et al.* 2023; González-Lara *et al*. 2025).

In the DTG curves, the free-water loss peak shifts from 100 °C in OPC to 105 °C and 110 °C in NS–PCE–OPC and Chitosan–NS–OPC, respectively, signifying stronger water binding. The C–S–H dehydration peak moves from 180 °C to 185 °C and 190 °C, and the portlandite dehydroxylation peak decreases from 480 °C in OPC to 470 °C and 460 °C, respectively, confirming accelerated CH consumption in the nano-silica blends. A minor shoulder near 300 °Cin both NS–PCE–OPC and Chitosan–NS–OPC corresponds to $Al(OH)_3$ dehydroxylation, implying formation of C–A–S–H and C–A–H phases. No significant DTG events around 700–750 °C were observed in any sample, indicating negligible $CaCO_3$ decomposition and minimal carbonation.

These results confirm that well-dispersed nano-silica (especially chitosan-grafted) provides additional C–S–H nucleation sites, consumes CH *via* pozzolanic reaction, and its polymer coating retards water evaporation, collectively accelerating hydration.

3.1.3 MIP Studies

Fig. 5 presents the cumulative and differential pore intrusion results from MIP measurements. The cementitious pore network is classified into five ranges: gel pores (< 0.01 µm), small (0.01–0.05 µm), medium (0.05–0.1 µm), large capillary pores (0.1–10 µm), and air voids (> 10 µm).

Incorporation of chitosan–modified nano-silica caused the intrusion to shift downward compared with those of OPC and NS–PCE–OPC. This reflects reductions in total intrusion of 26.0 % and 6.2 % for the Chitosan–NS–OPC mix compared to OPC and NS–PCE–OPC, respectively.

Moreover, the log differential intrusion data in show that, within the 0.1–10 µm pore size range, the Chitosan–NS–OPC sample displayed a flatter, plateau-like shape compared to the sharper peaks seen in the other mixes. This trend suggests that the pore size distribution in Chitosan–NS–OPC became more homogeneous. As for the pore size fractions, the gel pore content was calculated as 6.5 %, 7.9 %, and 12.4 % for OPC, NS–PCE–OPC, and Chitosan–NS–OPC, respectively. The increase in gel pores content in Chitosan–NS–OPC translates to gains of 90.8 % and 57.0 % over OPC and NS–PCE–OPC, respectively, signifying the development of additional gel-like hydration products. The fraction of small capillary pores increased from 19.5 % in OPC to 22.4 % in NS–PCE–OPC and 23.3 % in Chitosan–NS–OPC.

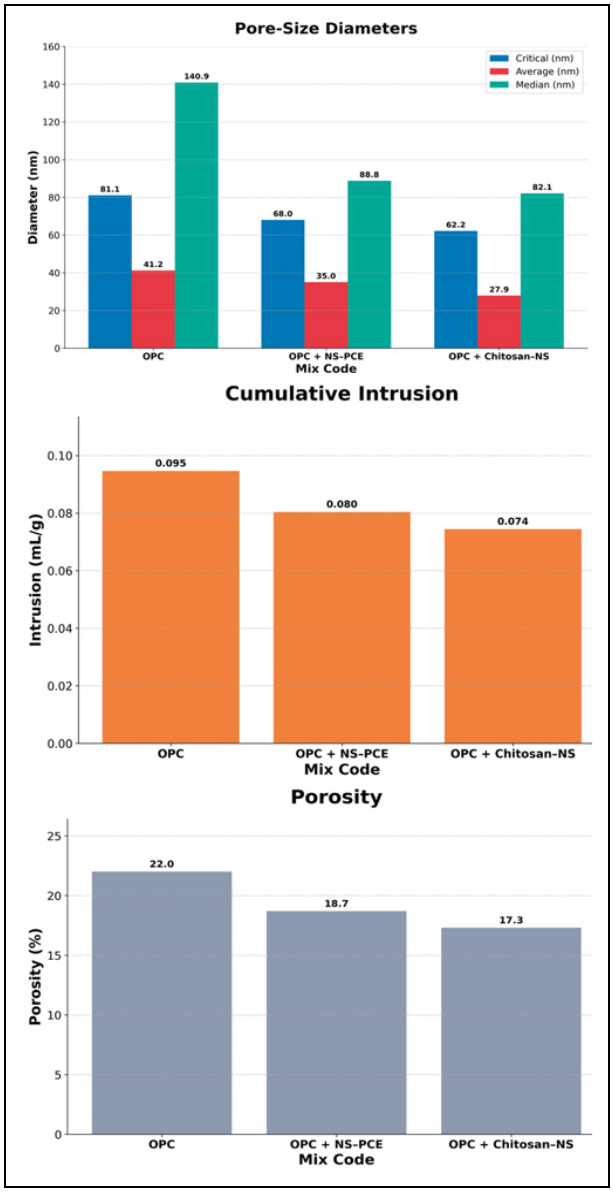


Fig. 5: Pore structure characteristics of mixed specimens

Medium capillary pores accounted for 19.5 %, 22.4 %, and 21.2 % in OPC, NS–PCE–OPC, and Chitosan–NS–OPC, respectively. Conversely, a significant reduction was observed in the fraction of large capillary pores, decreasing from 50.2 % and 44.6 % in OPC and NS–PCE–OPC, respectively, to 39.2 % in Chitosan–NS–OPC. These findings confirm that incorporating chitosan–modified nano-silica notably refined the pore structure by reducing the prevalence of large pores and increasing the proportion of harmless smaller pores. Such refinement enhances the densification of the pore network and is expected to improve the macroscopic durability of the composite, as large pores are known to be detrimental to performance (Mehta and Monteiro, 2006; Mindess, 2019).

Table 5. Pore structure parameters for mixed specimens

Mix Code	Critical Pore Diameter (nm)	Average Pore Diameter (nm)	Median Pore Diameter (nm)	Porosity (%)
OPC	81.1	41.2	140.9	22
OPC + NS–PCE	68	35	88.8	18.7
OPC + Chitosan–NS	62.2	27.9	82.1	17.3

Table 5 highlights the characteristic pore structure parameters. The critical pore diameter represents the size of pore throats most connected to permeability (Du *et al*. 2014). The critical pore diameter in Chitosan–NS–OPC was reduced to 62.2 nm, compared to 81.1 nm and 68.0 nm in OPC and NS–PCE–OPC, respectively, representing decreases of 23.3 % and 8.5 %. Additionally, Chitosan–NS–OPC exhibited an average pore diameter of 27.9 nm, markedly lower than the 41.2 nm in OPC and 35.0 nm in NS–PCE–OPC, with reductions of 32.3 % and 20.3 %, respectively. Similarly, the median pore diameter decreased to 82.1 nm in Chitosan–NS–OPC, from 140.9 nm and 88.8 nm in OPC and NS–PCE–OPC, indicating reductions of 41.7 % and 7.6 %, respectively. Furthermore, the overall porosity of Chitosan–NS–OPC was reduced to 17.3 %, compared to 22.0 % and 18.7 % in OPC and NS–PCE–OPC, corresponding to decreases of 21.4 % and 7.5 %. These results clearly demonstrate that the use of chitosan–modified nano-silica not only reduced pore size parameters but also narrowed their distribution, contributing to a denser and more uniform microstructure (Yu *et al*. 2014; Ecay *et al.* 2020).

The observed refinement in the pore structure of Chitosan–NS–OPC can be attributed to the synergistic effects of well-dispersed nano-silica particles and the chitosan biopolymer. The chitosan–modified nano-silica serves as nucleation sites for hydration products, creating additional gel phases (Beskopylny *et al*. 2022; Hamada *et al*. 2023; Kong *et al.* 2012), as reflected in the increased gel pores fraction. Furthermore, the deagglomerated nanoparticles effectively fill micro- and nanopores, enhancing particle packing and reducing the fraction of larger capillary pores. The pozzolanic activity of nano-silica also contributes by generating additional C–S–H gel, thus lowering overall porosity (Kooshkaki and Eskandari-Naddaf, 2019; Arif *et al.*, 2023).

3.1.4 SEM Analysis

Fig. 6 depicts the morphological characteristics of the test specimens. Interfacial transition zone (ITZ) between the cement pastes and aggregate is usually regarded as the weakest link in cement-based materials, substantially influencing the bulk properties (Kishore and Tomar, 2023). As illustrated in Fig. 6(a), the hydrated structure of the plain OPC mortar highlights the typical ITZ morphology, encompassing the sand particles and hydration products (notably CH and C–S–H gel), along with conspicuous voids and microcracks. In particular, the OPC specimen displayed a relatively porous and inhomogeneous microstructure with evident discontinuities in the hydration products, indicative of an incomplete degree of hydration. This microstructural deficiency adversely affected the overall mechanical and durability performance of the cementitious composite.

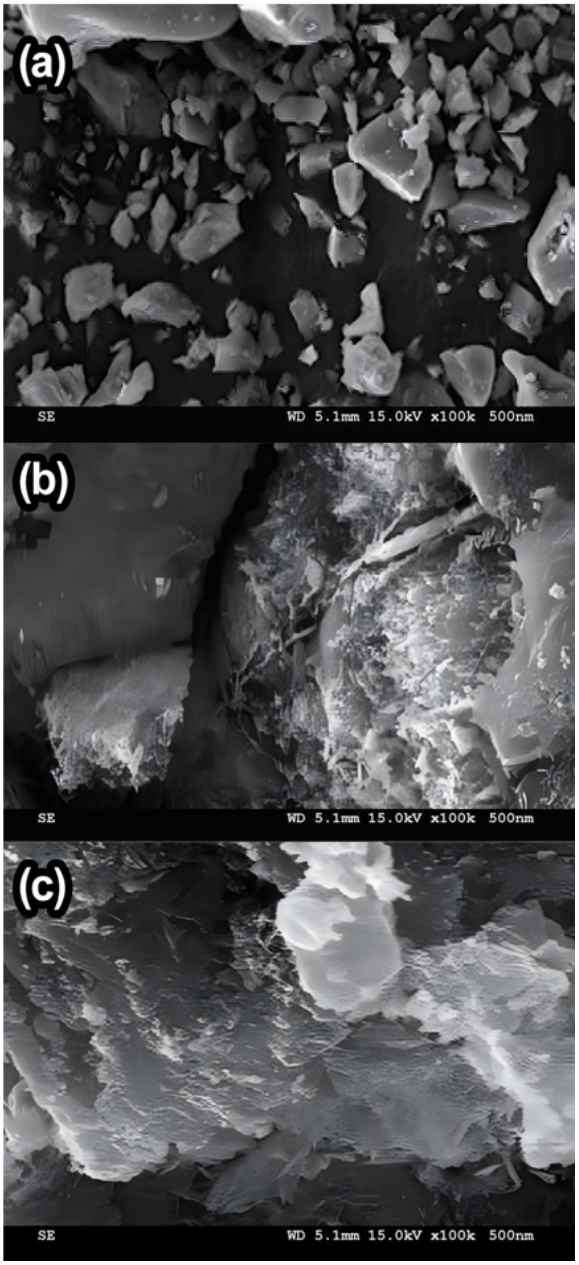


Fig. 6: SEM characterization of a) control (OPC), b) PCE-treated NS, and C) chitosan-treated NS

In contrast, as shown in Fig. 6(b), the incorporation of PCE-modified nanosilica significantly refined and densified the microstructure compared to the plain OPC matrix. The Nanosilica–PCE–OPC specimen revealed a more compact arrangement of hydration products, with improved adhesion between the sand grains and cementitious matrix at the ITZ. Nevertheless, occasional voids and air pockets were observed, likely arising from the water-retention and air-entraining behavior of the PCE, which attracts water and can inadvertently trap air bubbles during hydration. Similarly, Fig. 6(c) illustrates the microstructure of the Chitosan–Nanosilica–OPC specimen, which exhibited an even denser packing of hydration products, especially C–S–H gel, forming a highly homogeneous and well-bonded microstructure. Notably, in the Chitosan–Nanosilica–OPC mix, the ITZ showed an intimate bond between the paste and aggregate with virtually no visible voids. Furthermore, the microstructure was enveloped by an abundance of C–S–H gel, contributing to a coherent, continuous matrix with strong interparticle adhesion. The Chitosan–Nanosilica–OPC specimen displayed the most refined and compact microstructure among the three, suggesting that the chitosan-treated nanosilica imparted superior microstructural enhancement compared to PCE-modified nanosilica.

The improvement in the cementitious matrix for chitosan-dispersed nanosilica specimens is attributed to multiple synergistic mechanisms:

- Uniformly dispersed chitosan-modified nanosilica serves as nucleation sites for the precipitation and growth of hydration products, which proliferate into the pore space, ensuring a more homogeneous spatial distribution and a refined pore structure (Alqamish and Tamimi, 2021; Barbhuiya *et al*. 2020), thereby improving macroscopic performance.

- The deagglomeration of chitosan-treated nanosilica aids in filling nanoscale voids in the cement matrix, enhancing packing density and producing a denser, more impermeable microstructure (Kumar *et al*. 2020; Quercia *et al*. 2013).

- Chitosan-treated nanosilica enhances pozzolanic activity by consuming CH in the ITZ to form additional C–S–H, lowering CH content and improving paste–aggregate bonding (Xu *et al*. 2017; Liu *et al*. 2019).

- The viscosity-modifying properties of the chitosan biopolymer improve the cohesiveness of the mix, suppressing bleeding and segregation during setting and promoting uniform particle distribution and densification.

- The presence of chitosan also mitigates premature water loss during curing (Arslan *et al*. 2019; Lv, 2016), sustaining hydration reactions for longer durations and fostering further matrix densification. Finally, chitosan biopolymer further supports pore refinement. With its high molecular weight and water retention capability due to increased solution viscosity (Zhou *et al*. 2008; Román-Doval *et al*. 2023). Chitosan reduces water loss during curing (Liu *et al*. 2015; Elbahrawy and Rahim, 2017), thereby promoting more complete hydration and improved microstructural development.

3.2 Macroscale Performance Characteristics

3.2.1 Compressive strength

Fig. 7 presents the compressive strength of specimens cured at 28 and 90 Days. As expected, all mixtures showed a clear upward trend in strength from 28 to 90 days. Continued hydration of the cement clinker phases over time can be credited to the sustained pozzolanic activity of nanosilica in the modified mixtures. Together, these reactions led to the progressive precipitation of additional binding gels such as C–S–H, C–A–S–H, and C–A–H, which further densified and strengthened the cementitious matrix.

Among all the specimens, the Chitosan–Nanosilica–OPC mixture stood out, achieving significantly higher compressive strength at both curing ages compared to the others. For instance, at 90 days, the Chitosan–Nanosilica–OPC mix surpassed the plain OPC specimen by approximately 35.2%, and outperformed the Nanosilica–PCE–OPC mixture by around 12.8%. This highlights the substantial benefit of combining chitosan with nanosilica as a surface modifier for cement composites.

Table 6 summarizes the ANOVA results (F- and P-values) for the compressive strength data at 28 and 90 days. At the 5% significance level ($\alpha = 0.05$), both PCE-modified and chitosan-modified nanosilica mixtures yielded F-values higher than the critical value, with corresponding P-values below 0.05. This confirms that the strength enhancements in the modified mixtures were statistically significant compared to the OPC control.

These improvements can largely be explained by the more efficient dispersion and higher reactivity of the nanosilica particles when treated with chitosan. Several synergistic mechanisms were at play (Xiaohan *et al*. 2024; Farzadnia *et al*. 2015; Regalla, 2024). Firstly, the nano-sized particles effectively filled microvoids in the matrix, reducing porosity and promoting a denser microstructure. Secondly, the seeding effect of the well-dispersed nanosilica particles accelerated the nucleation

and development of hydration products, enhancing early and later-age strength development.

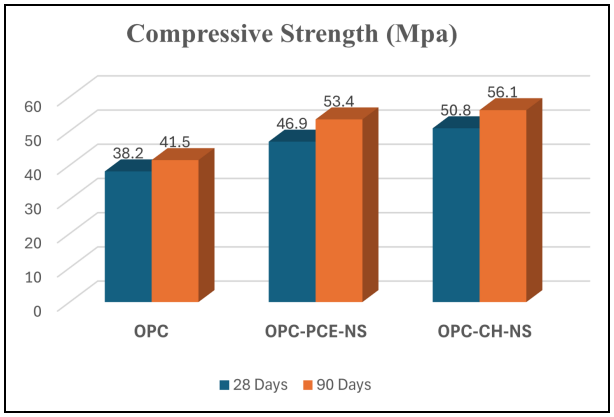


Fig. 7: Compressive strength of specimens at 28 and 90 days

Table 6. Compressive strength, UPV, electrical resistivity of OPC, nanosilica–PCE–OPC, and chitosan–nanosilica–OPC specimens at 28 and 90 days

Property	Age (days)	OPC	Nanosilica–PCE–OPC	Chitosan–Nanosilica–OPC
Compressive Strength (MPa)	28	38.2	46.9	50.8
	90	41.5	53.4	56.1
UPV (m/s)	28	3687	4549	4815
	90	3886	4971	5326
Electrical Resistivity (kΩ·cm)	28	17.6	20.2	22.6
	90	19.7	23.1	25.9
F-value (CS)	28	—	23.4	29.7
	90	—	25.6	32.1
P-value (CS)	28	—	0.004	0.002
	90	—	0.003	0.001
F-value (UPV)	28	—	19.2	27.8
	90	—	21.5	30.3
P-value (UPV)	28	—	0.006	0.002
	90	—	0.005	0.001
F-value (ER)	28	—	16.8	24.3
	90	—	18.9	26.7
P-value (ER)	28	—	0.008	0.003
	90	—	0.007	0.002

On top of these effects, the chitosan biopolymer imparted unique water-retention properties that benefited internal curing. The presence of chitosan helped sustain moisture availability in the microstructure for a longer time, facilitating the hydration of otherwise unreacted cement grains and enabling more hydration products to precipitate within the pore network (Kong *et al.* 2013; Chen *et al*. 2022). This delayed water release mechanism also helped to mitigate early-age shrinkage and reduce microcrack formation, contributing not only to strength but also to durability.

Taken together, these combined benefits rendered the Chitosan–Nanosilica–OPC specimen mechanically superior to its Nanosilica–PCE–OPC counterpart. This underscores the advantage of chitosan over conventional PCE as a dispersing agent for nanosilica in cement-based composites, particularly when the goal is to maximize strength development.

3.2.2 Ultrasonic Pulse Velocity (UPV) Measurements

The ultrasonic pulse velocity (UPV) measurements for the composites at 28 and 90 days are presented in Fig. 8. All mixtures exhibited increased UPV values with curing time, consistent with ongoing hydration and pozzolanic reactions in the modified specimens, which enhanced matrix density and uniformity. At 28 days, the UPV values for OPC, Nanosilica–PCE–OPC, and Chitosan–Nanosilica–OPC represented improvements of approximately 5.4%, 9.3%, and 10.6% over their respective 28-day values.

The Chitosan–Nanosilica–OPC specimen consistently recorded the highest UPV across all ages. At 90 days, the UPV of this mix exceeded that of OPC and Nanosilica–PCE–OPC by about 37.1% and 7.1%, respectively. ANOVA confirmed the significance of these improvements, with F-values exceeding the critical threshold and P-values < 0.05 at both curing ages (Table 6).

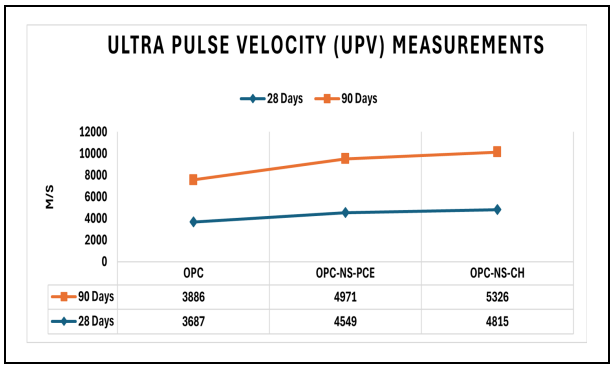


Fig. 8: UPV measurements of mix specimens

These gains reflect the synergistic contributions of the nanosilica, combined with the moisture-retention and crack-control functions of the chitosan biopolymer (Huang *et al.* 2024; Zhao *et al.* 2020). The resulting microstructure was denser and more homogeneous, enabling faster ultrasonic transmission. The mitigation of microcracks by chitosan further enhanced structural integrity and homogeneity, consistent with the trends observed in compressive strength (Section 3.2.1).

According to Whitehurst's classification (Whitehurst, 1951), the OPC mixture was rated as good

quality at both ages, while the Nanosilica–PCE–OPC and Chitosan–Nanosilica–OPC mixtures were classified as excellent, owing to their improved compactness and reduced heterogeneity.

3.2.3 Electrical Resistivity

Since the electrical resistivity of cementitious materials is strongly influenced by pore structure and connectivity, a non-destructive resistivity test was performed to evaluate the composites' resistance to ion penetration (Tang *et al.* 2016). Fig. 9 presents the electrical resistivity values of the specimens at different curing ages. All mixtures exhibited increasing resistivity over time, reflecting progressive microstructural refinement and reduced pore connectivity. At 90 days, the resistivity values of OPC, Nanosilica–PCE–OPC, and Chitosan–Nanosilica–OPC mixes were 19.7, 23.1, and 25.9 kΩ·cm, respectively, corresponding to increases of 12.2%, 14.3%, and 15.4% relative to their 28-day values.

Among the three, the Chitosan–Nanosilica–OPC specimen consistently showed the highest resistivity, 35.3% greater than OPC and 13.3% higher than Nanosilica–PCE–OPC at 90 days, indicating a more uniform and impermeable microstructure. This improvement is expected to enhance durability by limiting ion ingress, such as chlorides, and extending service life.

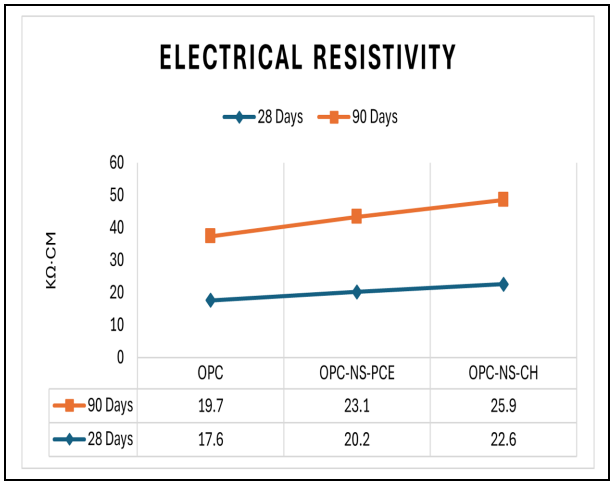


Fig. 9: Electrical resistivity measurements of mixed specimens

ANOVA analysis (Table 6) confirmed that chitosan- and PCE-assisted nanosilica significantly increased resistivity, with F-values exceeding Fcrit and P-values below 0.05 at both curing ages. Additionally, chitosan's ability to reduce shrinkage-induced microcracking (Zhao *et al.* 2024; Wang *et al.* 2023) further supports microstructural uniformity, corroborating trends observed in UPV (Section 3.2.2) and mechanical performance.

4. CONCLUSION

This study evaluated the effects of chitosan-treated nanosilica on cementitious composites using multi-scale experimental and statistical analyses, compared with PCE-treated nanosilica and plain OPC. Microscopic investigations revealed enhanced hydration, stronger pozzolanic activity, increased C–S–H formation, and a denser, refined pore structure with reduced porosity. Chitosan–nanosilica significantly decreased critical, average, and median pore diameters relative to OPC. These microstructural improvements translated to superior macroscopic performance, with higher compressive strength, UPV, electrical resistivity, and durability at 90 days. Additionally, chitosan improved internal curing, crack mitigation, and sustainability, demonstrating clear advantages over synthetic PCE.

FUNDING

This research received no specific grant from any funding agency in the public, commercial, or not-for-profit sectors.

CONFLICTS OF INTEREST

The authors declare that there is no conflict of interest.

COPYRIGHT

This article is an open-access article distributed under the terms and conditions of the Creative Commons Attribution (CC-BY) license (http://creativecommons.org/licenses/by/4.0/).

REFERENCES

Alqamish, H. H. and Tamimi, A. Al., Development and evaluation of nano-silica sustainable concrete, *Appl. Sci.*, 11(7), 3041 (2021). https://doi.org/10.3390/app11073041

ASTM C305-20 – Standard Practice for Mechanical Mixing of Hydraulic Cement Pastes and Mortars of Plastic Consistency, *American Society for Testing and Materials* (2020).

Aranaz, I., A., Alcántara, R. A., Civera, M. C., Arias, C., Elorza, B., Caballero, A. H., and Acosta, N., Chitosan: An overview of its properties and applications, *Polym.*, 13(19), 3256 (2021). https://doi.org/10.3390/polym13193256

Arif, M., Syed, D. H. and Salman, S., Effect of nanosilica on strength and permeability of concrete, Materials Today: Proceedings (2023). https://doi.org/10.1016/j.matpr.2023.04.073

Arslan, H., A., Aytaç, U. S., Bilir, T. and Şen, S., The synthesis of a new chitosan based superplasticizer and investigation of its effects on concrete properties, *Constr. Build. Mater.,* 204, 541-549 (2019). https://doi.org/10.1016/j.conbuildmat.2019.01.209

Bai, S., B., Guan, X., Li, H. and Ou, J., Effect of the specific surface area of nano-silica particle on the properties of cement paste, *Powder Technol.,* 392, 680-689 (2021). https://doi.org/10.1016/j.powtec.2021.07.045

Barbhuiya, G. H., Moiz, M. A., Hasan, S. D. and Zaheer, M. M., Effects of the nanosilica addition on cement concrete: A review, *Mater. Today Proc.,* 32, 560-566 (2020). https://doi.org/10.1016/j.matpr.2020.02.143

Beskopylny, A. N., Stel'makh, S. A., Shcherban', E. M., Mailyan, L. R., Meskhi, B., Varavka, V., Beskopylny, N. and El'shaeva, D., A Study on the Cement Gel Formation Process during the Creation of Nanomodified High-Performance Concrete Based on Nanosilica, *Gels*, 8(6), 346 (2022). https://doi.org/10.3390/gels8060346

Bi, S., Wang, M., Huang, L., Qin, D., Cheng, X. and Chen, X., Evaluation of structure transformation and biocompatibility of chitosan in alkali/urea dissolution system for its large-scale application, *Int. J. Biol. Macromol.,* 154, 758-764 (2020). https://doi.org/10.1016/j.ijbiomac.2020.03.075

Biricik, H., B. and Sarier, N., Comparative study of the characteristics of nanosilica-, silica fume-and fly ash-incorporated cement mortars, *Mater. Res*., 17, 570-582 (2014). https://doi.org/10.1590/s1516-14392014005000054

IS 13311(Part 1):1992 – Non-destructive Testing of Concrete – Methods of Test, Part 1: Ultrasonic Pulse Velocity. New Delhi: BIS (1992).

IS 383:2016 – Coarse and Fine Aggregate for Concrete – Specification (3rd revision). New Delhi: BIS (2016).

IS 4031 (Part 6):1988 – Methods of Physical Tests for Hydraulic Cement, Part 6: Determination of Compressive Strength of Hydraulic Cement (other than masonry cement). New Delhi: BIS (1988).

IS 650:1991 – Specification for Standard Sand for Testing of Cement. New Delhi: BIS (1991).

IS 8112:2013 – Specification for 43 Grade Ordinary Portland Cement. New Delhi: BIS (2013).

Chen, Y. X., Li, S., Mezari, B., Hensen, E.J., Yu, R., Schollbach, K., Brouwers, H. J. H. and Yu, Q., Effect of highly dispersed colloidal olivine nano-silica on early age properties of ultra-high performance concrete, *Cem. Concr. Compos*., 131, 104564 (2022). https://doi.org/10.1016/j.cemconcomp.2022.104564

Chong, J. Z., Sutan, N. M. and Yakub, I., Characterization of early pozzolanic reaction of calcium hydroxide and calcium silicate hydrate for nanosilica modified cement paste, *J. Civil Eng. Sci. Technol.,* 4(3), 6-10 (2013). https://doi.org/10.33736/jcest.120.2013

Dong, P., Allahverdi, A., Andrei, C. M. and Bassim, N. D., The effects of nano-silica on early-age hydration reactions of nano Portland cement, *Cem. Concr. Compos*., 133, 104698 (2022). https://doi.org/10.1016/j.cemconcomp.2022.104698

Doval, R. Ramón, Arellanes, -T. P. S., Barajas, -T. Y. A., Sánchez, -G. A. and Lazcano, -V. A. A., Chitosan: Properties and its application in agriculture in context of molecular weight, *Polym.,* 15(13), 2867 (2023). https://doi.org/10.3390/polym15132867

Du, H., D., Du, S. and Liu, X., Durability performances of concrete with nano-silica, *Constr. Build. Mater.,* 73, 705-712 (2014). https://doi.org/10.1016/j.conbuildmat.2014.10.014

Du, S., Wu, J., AlShareedah, O. and Shi, X., Nanotechnology in cement-based materials: A review of durability, modeling, and advanced characterization, *Nanomater*., 9(9), 1213 (2019). https://doi.org/10.3390/nano9091213

Ecay, L., Grégoire, D. and Cabot, -P. G., On the prediction of permeability and relative permeability from pore size distributions, *Cem. Concr. Res*., 133, 106074 (2020). https://doi.org/10.1016/j.cemconres.2020.106074

Elbahrawy, S, M. E., R. A. and Rahim, A., Effect of addition of chitosan on water sorption, solubility and microhardness of glass ionomer cement, *Tanta Dent. J*., 14(3), 164-168 (2017). https://doi.org/10.4103/tdj.tdj_26_17

Farzadnia, N., Noorvand, H., Yasin, M. A., and Aziz, F. N. A., The effect of nanosilica on short-term drying shrinkage of POFA cement mortars, *Construct. Build. Mater*., 95, 636-646 (2015). https://doi.org/10.1016/j.conbuildmat.2015.07.132

Feng, P., Chang, H., Liu, X., Ye, S., Shu, X. and Ran, Q., The significance of dispersion of nano-SiO2 on early age hydration of cement pastes, *Mater. Design*, 186 108320 (2020). https://doi.org/10.1016/j.matdes.2019.108320

Garcia, -E. J. I., Non-evaporable water from neat OPC and replacement materials in composite cements hydrated at different temperatures, *Cem. Concr. Res*., 33(11), 1883-1888 (2003). https://doi.org/10.1016/s0008-8846(03)00208-4

Golewski, L. G., Combined effect of coal fly ash (CFA) and nanosilica (nS) on the strength parameters and microstructural properties of eco-friendly concrete, *Energ*., 16(1), 452 (2022). https://doi.org/10.3390/en16010452

Hamada, H., Shi, J., Yousif, T. S., Jawahery, A. M., Tayeh, B. and Jokhio, G., Use of nano-silica in cement-based materials–a comprehensive review, *J. Sustainable Cem.-Based Mater*., 12(10), 1286-1306 (2023). https://doi.org/10.1080/21650373.2023.2214146

Heikal, M., Aleem, E. A. S. and Morsi, M. W., Characteristics of blended cements containing nano-silica, *HBRC J*., 9(3), 243-255 (2013). https://doi.org/10.1016/j.hbrcj.2013.09.001

Hou, P., Qian, J., Cheng, X. and Shah, P. S., Effects of the pozzolanic reactivity of nanoSiO2 on cement-based materials, *Cem. Concr. Compos*., 55, 250-258 (2015). https://doi.org/10.1016/j.cemconcomp.2014.09.014

Huang, F., Rong, S., Tao, S., Chu, H., Huang, H., Gao, S., Zhang, X., Xiong, X. and Zhang, C., A novel chitosan/biochar-modified eco-concrete with balanced mechanical, planting, and water purification performance for riparian restoration, *J. Cleaner Prod*., 481, 144144 (2024). https://doi.org/10.1016/j.jclepro.2024.144144

Iqbal, S., Pan, G., Meng, H., Sun, H., Liu, B. and Zhou, F., Surfactant-free synthesis of highly monodispersed in situ grown nano-silica on modified fly ash and its impact on the properties of cement pastes, *Construct. Build. Mater.*, 425, 136043 (2024). https://doi.org/10.1016/j.conbuildmat.2024.136043

Jafarbeglou, M., Abdouss, M. and Ramezanianpour, A. A., Nanoscience and nano engineering in concrete advances, a review, *Int. J. Nanosci. Nanotechnol.,* 11(4), 263-273 (2015).

Jahangir, S. and Kazemi, S., Effect of nano-alumina (N-Al) and nanosilica (NS) as admixtures on concrete behavior, *In Int. Conf. Adv. Agric. Biol. Environ. Sci.,*37-41(2014). https://doi.org/10.15242/iicbe.c1014078

Jain, J. and Neithalath, N., Analysis of calcium leaching behavior of plain and modified cement pastes in pure water, *Cem. Concr. Compos.,* 31(3), 176-185 (2009). https://doi.org/10.1016/j.cemconcomp.2009.01.003

Jiang, C., Jiang, L., Tang, X., Gong, J. and Chu, H., Impact of calcium leaching on mechanical and physical behaviors of high belite cement pastes, *Construc. Build. Mater*., 286, 122983 (2021). https://doi.org/10.1016/j.conbuildmat.2021.122983

Jonnala, S. N., Gogoi, D., Devi, S., Kumar, M. and Kumar, C., A comprehensive study of building materials and bricks for residential construction, *Construc. Build. Mater.,* 425, 135931 (2024). https://doi.org/10.1016/j.conbuildmat.2024.135931

Joseph, S., Skibsted, J. and Cizer, Ö., A quantitative study of the C3A hydration, *Cem. Concr. Res*., 115, 145-159 (2019). https://doi.org/10.1016/j.cemconres.2018.10.017

Kandasamy, A., Ramesh, B., Khazaleh, A. M. and Sabari, K., Evaluating the Microstructure and Strength of Geopolymer Mud Blocks for Sustainable Architecture, *Civil Eng. J.,* 11(4), 1410–1431 (2025b). https://doi.org/10.28991/CEJ-2025-011-04-09

Kandasamy, A., Ramesh, B., Khazaleh, M. A., and Athiappan, K., Behavior of High-performance Geopolymer Concrete Beams with Substitution of Silica Fume and GGBS/Fly Ash*, J. Environ. Nano technol.,* 14(1), 52–62 (2025c). https://doi.org/10.13074/jent.2025.03.2511289

Kandasamy, A., Rachel, P. P., Khazaleh, M. A., and Athiappan, K., Comparative Analysis on Load-deformation Behavior of RC Slabs Incorporating Nano-SiO2 and Coconut Fibers, *J. Environ. Nanotechnol*., 14(1), 18–29 (2025a). https://doi.org/10.13074/jent.2025.03.2511233

Khan, K., Ahmad, W., Amin, M. N. and Nazar, S., Nano-silica-modified concrete: A bibliographic analysis and comprehensive review of material properties, *Nanomater.,* 12(12), 1989 (2022). https://doi.org/10.3390/nano12121989

Kim, K. -M., Heo, Y. -S., Kang, S. -P. and Lee, J., Effect of sodium silicate-and ethyl silicate-based nano-silica on pore structure of cement composites, *Cem. Concr. Compos*., 49, 84-91 (2014). https://doi.org/10.1016/j.cemconcomp.2013.12.009

Kishore, K. and Tomar, R., Understanding the role of interfacial transition zone in cement paste and concrete, *Mater. Today Proc*., 80, 877-881 (2023). https://doi.org/10.1016/j.matpr.2022.11.322

Kong, D., Du, X., Wei, S., Zhang, H., Yang, Y. and Shah, P. S., Influence of nano-silica agglomeration on microstructure and properties of the hardened cement-based materials, *Construct. Build. Mater*., 37, 707-715 (2012). https://doi.org/10.1016/j.conbuildmat.2012.08.006

Kong, D., Su, Y., Du, X., Yang, Y., Wei, S. and Shah, S.P., Influence of nano-silica agglomeration on fresh properties of cement pastes, *Construct. Build. Mater*., 43, 557-562 (2013). https://doi.org/10.1016/j.conbuildmat.2013.02.066

Kooshkaki, A. and Naddaf, E. H., Effect of porosity on predicting compressive and flexural strength of cement mortar containing micro and nano-silica by multi-objective ANN modeling, *Construct. Build. Mater.,* 212, 176-191 (2019). https://doi.org/10.1016/j.conbuildmat.2019.03.243

Korayem, A. H., Tourani, N., Zakertabrizi, M., Sabziparvar, A. M. and Duan, W. H., A review of dispersion of nanoparticles in cementitious matrices: Nanoparticle geometry perspective, *Construct. Build. Mater.,* 153, 346-357 (2017). https://doi.org/10.1016/j.conbuildmat.2017.06.164

Kumar, K. S. J., Rao, S. M. V., Reddy, S. V. and Shrihari, S., Performance evaluation of nano-silica concrete, *In E3S Web of Conf*., 184, 01076 (2020). https://doi.org/10.1051/e3sconf/202018401076

Lara, -G. H., Pacheco, -P, B., García, -R. E., Becerra, -A. H., Pérez, -F. A. A. and Trejo, -G. F. J., Black Soldier Fly Culture as a Source of Chitin and Chitosan for Its Potential Use in Concrete: An Overview, *Polym*., 17(6), 17060717 (2025). https://doi.org/10.3390/polym17060717

Li, R., Chen, W. C., Lei, L. and Plank, J., Dispersing efficacy of tailored IPEG PCEs in AAS binders: elucidating the impact of PCE molecular weight, *Ind. Eng. Chem. Res*., 62(4), 1776-1787 (2023a). https://doi.org/10.1021/acs.iecr.2c03820

Li, Y., Duan, C., Meng, M., Zhang, J., Huang, H., Wang, H., Yan, M., Tang, X. and Huang, X., Effect of clay minerals on polycarboxylate superplasticizer and methods to improve the performance of concrete containing clay: a review, *J. Mater. Sci*., 58(39), 15294-15313 (2023b). https://doi.org/10.1007/s10853-023-08989-0

Li, Y., Mi, T., Liu, W., Dong, Z., Dong, B., Tang, L. and Xing, F., Chemical and mineralogical characteristics of carbonated and uncarbonated cement pastes subjected to high temperatures, *Compos. Part B: Eng.,* 216, 108861 (2021). https://doi.org/10.1016/j.compositesb.2021.108861

Liu, B., Wang, L., Pan, G. and Li, D., Dispersion of graphene oxide modified polycarboxylate superplasticizer in cement alkali solution for improving cement composites, *J. Build. Eng*., 57, 104860 (2022). https://doi.org/10.1016/j.jobe.2022.104860

Liu, H., Bu, Y., Sanjayan, J. and Shen, Z., Effects of chitosan treatment on strength and thickening properties of oil well cement, *Construct. Build. Mater.,* 75, 404-414 (2015). https://doi.org/10.1016/j.conbuildmat.2014.11.047

Liu, R., Xiao, H., Liu, J., Guo, S. and Pei, Y., Improving the microstructure of ITZ and reducing the permeability of concrete with various water/cement ratios using nano-silica, *J. Mater. Sci.,* 54(1), 444-456 (2019). https://doi.org/10.1007/s10853-018-2872-5

Lu, J., Jiang, J., Lu, Z., Li, J., Niu, Y. and Yang, Y., Pore structure and hardened properties of aerogel/cement composites based on nanosilica and surface modification, *Construct. Build. Mater.,* 245, 118434 (2020). https://doi.org/10.1016/j.conbuildmat.2020.118434

Lv, S. H., High-performance superplasticizer based on chitosan, *In Biopolym. biotech admixtures for eco-effic. Constr. Mater*., X(X), 131-150 (2016). https://doi.org/10.1016/b978-0-08-100214-8.00007-5

Maach, N., Georgin, J. F., Berger, S. and Pommay. J., Chemical mechanisms and kinetic modeling of calcium aluminate cements hydration in diluted systems: Role of aluminium hydroxide formation, *Cem. Concr. Res*., 143, 106380 (2021). https://doi.org/10.1016/j.cemconres.2021.106380

Mehta, P. K. and Monteiro, J. M. P., Concrete: microstructure, properties, and materials, (McGraw-Hill Publishing, (2006).

Mindess, S., ed., Developments in the Formulation and Reinforcement of Concrete, *Woodhead Publishing*, (2019). https://doi.org/10.1016/10.1016/C2017-0-03347-5

Mustapha, S., Ndamitso, M. M., Abdulkareem, A. S., Tijani, J. O., Shuaib, D. T., Mohammed, A. K. and Sumaila, A., Comparative study of crystallite size using Williamson-Hall and Debye-Scherrer plots for ZnO nanoparticles, *Adv. Nat. Sci.: Nanosci. Nanotechnol*., 10(4), 045013 (2019). https://doi.org/10.1088/2043-6254/ab52f7

Naddaf, M., Kafa, H. and Ghanem, I., Extraction and characterization of nano-silica from olive stones, *Silicon*, 12, 185-192 (2020). https://doi.org/10.1007/s12633-019-00112-w

Nicolle, L., Journot, C. M. A. and Lemaire, -G. S., Chitosan functionalization: Covalent and non-covalent interactions and their characterization, *Polym*., 13(23), 4118 (2021). https://doi.org/10.3390/polym13234118

Qian, Y., Lesage, K., Cheikh, E. K. and Schutter, G. D., Effect of polycarboxylate ether superplasticizer (PCE) on dynamic yield stress, thixotropy and flocculation state of fresh cement pastes in consideration of the Critical Micelle Concentration (CMC), *Cem. Concr. Res.,* 107, 75-84 (2018). https://doi.org/10.1016/j.cemconres.2018.02.019

Quercia, G., Lazaro, A., Geus, J. W. and Brouwers, H. J. H., Characterization of morphology and texture of several amorphous nano-silica particles used in concrete, *Cem. Concr. Compos*., 44, 77-92 (2013). https://doi.org/10.1016/j.cemconcomp.2013.05.006

Rahmani, S., Sharif, A. and Korayem, H. A., Dispersion stability of chitosan grafted graphene oxide nanosheets in cementitious environments and their effects on the fluidity of cement mortar nanocomposites, *J. Appl. Polym. Sci*., 139(19), 52095 (2022). https://doi.org/10.1002/app.52095

Rath, B., Praveenkumar, TR., Dhami, K. S., Paramasivam, P. and Yusuf, M., Sustainable LC3 Concrete in the Circular Economy: Assessment of Mechanical, Microstructural, and Durability Characteristics with Surkhi, Metakaolin, Nano-Silica, and M-Sand Blended Concrete, *Global Challenges*, 9(5), 2500026 (2025). https://doi.org/10.1002/gch2.202500026

Regalla, S. S. and N, S. K., Effect of nano SiO2 on rheology, nucleation seeding, hydration mechanism, mechanical properties and microstructure amelioration of ultra-high-performance concrete, *Case Stud. Constr. Mater*., 20, e03147 (2024). https://doi.org/10.1016/j.cscm.2024.e03147

Ren, C., Hou, L., Li, J., Lu, Z. and Niu, Y., Preparation and properties of nanosilica-doped polycarboxylate superplasticizer, *Constr. Build. Mater.,* 252, 119037 (2020). https://doi.org/10.1016/j.conbuildmat.2020.119037

Rupasinghe, M., Nicolas, R. S., Mendis, P., Sofi, M. and Ngo, T., Investigation of strength and hydration characteristics in nano-silica incorporated cement paste, *Cem. Concr. Compos*., 80, 17-30 (2017). https://doi.org/10.1016/j.cemconcomp.2017.02.011

Safiuddin, Md, Gonzalez, M., Cao, J. and Tighe, S. L., State-of-the-art report on use of nano-materials in concrete, *Int. J. Pavement Eng*., 15(10), 940-949 (2014). https://doi.org/10.1080/10298436.2014.893327

Saleh, N. J., Ibrahim, I. R. and Salman, D. A., Characterization of nano-silica prepared from local silica sand and its application in cement mortar using optimization technique, *Adv. Powder Technol*., 26(4), 1123-1133 (2015). https://doi.org/10.1016/j.apt.2015.05.008

Scrivener, K., Snellings, R. and Lothenbach, B., A practical guide to microstructural analysis of cementitious materials, 1st Ed., *CRC press*, 1-560 (2016). https://doi.org/10.1201/b19074

Singh, A., Sharma, T., Trivedi, J. and Chaturvedi, R. K., "Effect of silica nanoparticles on crude oil emulsions stabilized by a natural surfactant from Fenugreek Seeds and polyacrylamide for subsurface oil mobilization applications." Colloids and Surfaces A: Physicochemical and Engineering Aspects 702 (2024): 135084. https://doi.org/10.1016/j.colsurfa.2024.135084

Song, H. and Li, X., An overview on the rheology, mechanical properties, durability, 3D printing, and microstructural performance of nanomaterials in cementitious composites, *Mater*., 14(11), 2950 (2021). https://doi.org/10.3390/ma14112950

Stepkowska, E. T., Hypothetical transformation of Ca (OH) 2 into CaCO 3 in solid-state reactions of portland cement, *J. Therm. Anal. Calorimet*., 80, 727-733 (2005). https://doi.org/10.1007/s10973-005-0721-7

Tang, S. W., Cai, X. H., He, Z., Zhou, W., Shao, H. Y., Li, Z. J., Wu, T. and Chen, E., The review of pore structure evaluation in cementitious materials by electrical methods, *Constr. Build. Mater*., 117, 273-284 (2016). https://doi.org/10.1016/j.conbuildmat.2016.05.037

Tsampali, E., Tsardaka, E. C., Pavlidou, E, Paraskevopoulos, K. M. and Stefanidou, M., Comparative study of the properties of cement pastes modified with nano-silica and Nano-Alumina, *Solid State Phenomena,* 286, 133-144 (2019). https://doi.org/10.4028/www.scientific.net/ssp.286.133

Tyukova, I. S., Safronov, A. P., Kotel'Nikova, A. P. and Agalakova, Y. D., Electrostatic and steric mechanisms of iron oxide nanoparticle sol stabilization by chitosan, *Polym. Sci. Series A.,* 56, 498-504 (2014). https://doi.org/10.1134/s0965545x14040178

Wang, J., Liao, J., Kong, X. and Yin, J., Characterization of the nanoparticles formed in aqueous phase of hydrating cement pastes in the presence of PCEs, *Cem. Concr. Res*., 165, 107086 (2023a). https://doi.org/10.1016/j.cemconres.2022.107087

Wang, L., Zhibin, Q., Wu, J., Sheng, G., Wang, H., Liu, K., Dong, X., Wang, F. and Jiang, J., Effect of Citric Acid-Modified Chitosan on Hydration Regulation and Mechanism of Composite Cementitious Material System, *Build.,* 14(1), 41 (2023b). https://doi.org/10.3390/buildings14010041

Wang, Q., Li, S., Pan, S., Cui, X., Corr, J. D. and Shah, P. S., Effect of graphene oxide on the hydration and microstructure of fly ash-cement system, *Constr. Build. Mater*., 198, 106-119 (2019). https://doi.org/10.1016/j.conbuildmat.2018.11.199

Whitehurst, E. A., Soniscope tests concrete structures, In J. *Proc*., 47(2), 433-444 (1951). https://doi.org/10.14359/12004

Wu, C. -R., Hong, Z. -Q., Yin, Y, -H. and Kou, S. -C., Mechanical activated waste magnetite tailing as pozzolanic material substitute for cement in the preparation of cement products, *Constr. Build. Mater*., 252, 119129 (2020). https://doi.org/10.1016/j.conbuildmat.2020.119129

Xiaohan, Z., Ahmad, J., Jebur, Y. M. and Deifalla, A. F., A review on partial substitution of nanosilica in concrete, *Rev. Adv. Mater. Sci*., 63(1), 20230157 (2024). https://doi.org/10.1515/rams-2023-0157

Xu, J., Wang, B. and Zuo, J., Modification effects of nanosilica on the interfacial transition zone in concrete: A multiscale approach, *Cem. Concr. Compos*., 81, 1-10 (2017). https://doi.org/10.1016/j.cemconcomp.2017.04.003

Xu, Z., Zhou, Z., Du, P. and Cheng, X., Effects of nano-silica on hydration properties of tricalcium silicate, *Constr. Build. Mater*., 125, 1169-1177 (2016). https://doi.org/10.1016/j.conbuildmat.2016.09.003

Yang, T., Liu, B., Li, L., Gan, X., Lu, L. and Li, Y., Agglomeration behavior of colloidal nano-silica and its effect on pore structure, mechanical properties and shrinkage of cement mortar, *Constr. Build. Mater*., 409, 133865 (2023). https://doi.org/10.1016/j.conbuildmat.2023.133865

Yehia, S., Ibrahim, A. M. and Ahmed, D. F., The impact of using natural waste biopolymer cement on the properties of traditional/fibrous concrete, *Inno. Infrastruct. Solut*., 8(11), 287 (2023). https://doi.org/10.1007/s41062-023-01253-z

Yim, H. J., Lee, H. and Kim, J. H., Evaluation of mortar setting time by using electrical resistivity measurements, *Constr. Build. Mater*., 146, 679-286 (2017). https://doi.org/10.1016/j.conbuildmat.2017.04.088

Yu, R., Spiesz, P. and Brouwers, H. J. H., Effect of nano-silica on the hydration and microstructure development of Ultra-High Performance Concrete (UHPC) with a low binder amount, *Constr. Build. Mater*., 65, 140-150 (2014). https://doi.org/10.1016/j.conbuildmat.2014.04.063

Zhao, H., Hu, Y., Tang, Z., Wang, K., Li, Y. and Li, W., Deterioration of concrete under coupled aggressive actions associated with load, temperature and chemical attacks: A comprehensive review, *Constr. Build. Mater*., 322, 126466 (2022). https://doi.org/10.1016/j.conbuildmat.2022.126466

Zhao, L., Guo, X., Liu, Y., Ge, Y., Guo, L., Shu, X. and Liu, J., Synergistic effects of silica nanoparticles/polycarboxylate superplasticizer modified graphene oxide on mechanical behavior and hydration process of cement composites, *RSC adv*.., 7(27), 16688-16702 (2017). https://doi.org/10.1039/c7ra01716b

Zhao, L., Wang, M., Zhang, L. and Sadeghzadeh, S. M., Impact of chitosan extracted from shrimp shells on the shrinkage and mechanical properties of cement-based composites using dendritic fibrous nanosilica, *Heliyon*., 10(11), e31576 (2024). https://doi.org/10.1016/j.heliyon.2024.e31576

Zhao, S., Liu, Z., Mu, Y., Wang, F. and He, Y., Effect of chitosan on the carbonation behavior of γ-C2S, *Cem. Concr. Compos.,* 111, 10367 (2020). https://doi.org/10.1016/j.cemconcomp.2020.103637

Zhou, H. Y., Chen, X. G., Kong, M., Liu, C. S., Cha, D. S. and Kennedy, J. F., Effect of molecular weight and degree of chitosan deacetylation on the preparation and characteristics of chitosan thermosensitive hydrogel as a delivery system, *Carbohy. Polym.,* 73(2), 265-273 (2008). https://doi.org/10.1016/j.carbpol.2007.11.026